Scripta Materialia 124 (2016) 160–163

Contents lists available at ScienceDirect

Scripta Materialia

journal homepage: www.elsevier.com/locate/scriptamat

Regular Article

Stabilization of nanocrystalline alloys at high temperatures *via* utilizing high-entropy grain boundary complexions

Naixie Zhou [1], Tao Hu [1], Jiajia Huang, Jian Luo *

Department of NanoEngineering; Program of Mater. Sci. Eng., University of California, San Diego, La Jolla, CA 92093, USA

ARTICLE INFO

Article history:
Received 15 June 2016
Received in revised form 9 July 2016
Accepted 9 July 2016
Available online 20 July 2016

Keywords:
Grain boundary segregation
Multicomponent alloying
High-entropy effect
Nanocrystalline alloy
Thermal stability

ABSTRACT

Multicomponent alloying can be utilized to enhance the thermal stability of nanocrystalline alloys. The grain boundary energy can be reduced significantly *via* both bulk and grain-boundary high-entropy effects with increasing temperature at/within the solid solubility limit, thereby reducing the thermodynamic driving force for grain growth. Moreover, grain boundary migration can be hindered by sluggish kinetics. To test these new theories, numerical experiments were conducted; subsequently, several nanoalloys, including a Ni-based alloy ($Ni_{80}Mo_{6.6}Ti_6Nb_6Ta_{1.4}$) and Ni-containing high-entropy alloys ($Ni_{29}Fe_{23}Co_{23}Cr_{23}Zr_2$ and $Ni_{25}Fe_{23}Co_{23}Cr_{23}Mo_2Nb_2Zr_2$), were designed and fabricated to demonstrate outstanding thermal stabilities that outperform the Ni-based binary nanocrystalline alloys.

Although nanocrystalline metals can exhibit superior properties such as high strength and hardness [1–4], their applications are often hindered by the extreme susceptibility to grain growth. For example, nanocrystalline Al, Sn, Pb, and Mg are subjected to grain growth even at room temperature [5–7]. There are two general approaches to stabilize nanocrystalline materials against grain growth [8–11]. First, kinetic stabilization by the solute-drag effects and/or Zener (particle) pinning can slow down grain boundary (GB) migration [12–14], which become less effective at high temperatures. Second, thermodynamic stabilization can be achieved by reducing the GB energy (γ_{GB}) *via* solute segregation (*a.k.a.* GB adsorption) to reduce the thermodynamic driving force for grain growth. Specifically, Weismuller originally proposed that an "equilibrium" grain size can be reached when the effective γ_{GB} vanishes [15,16]. Yet, Kirchheim [17] showed that the equilibrium-grain-size binary nanocrystalline alloys generally represent metastable states in supersaturated regions if (and only if) the precipitation is hindered kinetically. In such cases, the kinetic inhibition of the precipitation also becomes more difficult with increasing temperature, triggering abrupt grain growth. These challenges motivate the present study to develop and test new theories and strategies to enhance the thermal stability of nanocrystalline alloys at high temperatures *via* utilizing high-entropy GB complexions (where the term "complexion" refers to an interfacial "phase" that is thermodynamically two-dimensional [18]).

Experimentally, stabilization of nanocrystalline alloys (nanoalloys) have been achieved in several binary systems, including Pd-Zr [19], W-Ti [20], Fe-Zr [21,22], and Cu-Zr [23] (where the primary phases are underlined). Li et al. also showed that addition of 1–4 at.% Hf could further enhance the thermal stability of the binary Fe-Zr alloys [24]. Specifically, an electrodeposited $Ni_{79}W_{21}$ nanoalloy was found to be stable up to 600–700 °C [25], which represents the best reported result for Ni-based nanoalloys. To test the proposed new strategies, this study demonstrated the stabilities of a Ni-based alloy ($Ni_{80}Mo_{6.6}Ti_6Nb_6Ta_{1.4}$) and two Ni-containing high-entropy alloys ($Ni_{29}Fe_{23}Co_{23}Cr_{23}Zr_2$ and $Ni_{25}Fe_{23}Co_{23}Cr_{23}Mo_2Nb_2Zr_2$) up to ~1000 °C, representing a noteworthy improvement from the binary Ni-based nanoalloys reported previously.

The Gibbs adsorption theory states:

$$d\gamma_{GB} = S^{XS}dT - \sum_i \Gamma_i d\mu_i \quad (1)$$

where S^{XS} (entropy) and Γ_i (adsorption) are the GB excess quantities, T is temperature, and μ_i is the chemical potential of the i-th element. Eq. (1) implies that the GB energy (γ_{GB}) can be reduced by segregation at a constant T and this effect can be enhanced for multicomponent (high-entropy) GBs under certain conditions. We should note that generally $(\partial\gamma_{GB}/\partial T)_{P,X_i} > 0$ for a specimen of a constant bulk composition (X^i_{Bulk}) due to thermally-induced desorption. In a recent article [26], we proposed that a high-entropy GB effect can be achieved for a saturated specimen (in equilibrium with precipitates), when the bulk composition moves long the solvus line, where the solutes' bulk chemical potentials are pinned by the precipitates so that $(\partial\gamma_{GB}/\partial T)_{P,X^i_{Bulk}\ \text{on solvus}} \approx (\partial\gamma_{GB}/\partial T)_{P,\mu_i} = -S^{XS}$; thus, γ_{GB} can be reduced with increasing temperature for a high-entropy GB with positive and

* Corresponding author.
E-mail address: jluo@alum.mit.edu (J. Luo).
[1] Contributed equally to this work.

http://dx.doi.org/10.1016/j.scriptamat.2016.07.014
1359-6462/

large S^{XS} [26]. This high-entropy GB effect has been verified by modeling [26]; however, realization of this strategy for a Ni-based alloy with common segregating elements like Zr, Nb, Ta, Mo, and W would require adding a substantial amount of total non-FCC alloying elements that often leads to a large amount of precipitates and/or formation of ordered phases, which complicates the explanation. Thus, we propose two new strategies *via* using a bulk high-entropy effect (that can occur in conjunction with the GB high-entropy effect) and sluggish kinetics in this study.

As one new strategy to stabilize nanoalloys at high temperatures, we propose that the coupling between bulk high-entropy effects (*e.g.*, high-entropy matrix NiFeCoCr) and the effect of including one (or more) strong GB segregating element(s) (*e.g.*, Zr) can effectively reduce γ_{GB} as the driving force for grain growth, and this effect can occur concurrently with the high-entropy GB effect proposed in Ref. [26] (*e.g.*, introducing additional GB segregating elements like Nb and Mo) to enhance one another. This bulk high-entropy effect is consequence of a competition between GB segregation and bulk precipitation. Specifically, precipitation limits GB segregation. The mixing entropy can effectively lower the free energy of the bulk high-entropy phase with respect to precipitates, thereby increasing the solid solubility of individual segregating elements to allow more reduction in γ_{GB} within the solubility limit.

To examine the above hypotheses, we conducted numerical experiments using a statistical thermodynamic model for multicomponent GB adsorption [26] that is a generalization of the binary Wynblatt-Chatain model [27]; this multicomponent model, as well as a few simplifications adopted, was derived and discussed in the Supplementary Material and it was briefly described (in a more general form) in Ref. [26]. Assuming ideal mixing (as a simplification, which is discussed in the Supplementary Material), the equilibrium GB composition of an *N*-component alloy can be obtained *via* a McLean-Langmuir type adsorption equation:

$$\frac{X^i_{GB}}{X^1_{GB}} = \frac{X^i_{Bulk}}{X^1_{Bulk}} \exp\left(-\frac{\Delta h_{ads.(i\to 1),0}}{kT}\right) \tag{2}$$

where X^i_{GB} and X^i_{Bulk} are the GB and bulk compositions (atomic fractions), respectively, of the *i*-th element/component ($i = 1, 2, \ldots N$), $\Delta h_{ads.(i\to 1),0}$ is the GB adsorption (segregation) enthalpy (*i.e.*, the enthalpic change of swapping one atom of the *i*-th element inside the bulk material with one atom of the first element at the GB, where the "0" in the subscript denotes ideal mixing, which is a simplification adopted here to focus our numerical experiments on the bulk and GB entropic effects instead of the non-ideal interactions), and *k* is the Boltzmann constant. The GB energy can be expressed as:

$$\gamma_{GB} = \gamma^{(0)}_{GB} - 2n\sum_{i\neq 1} X^i_{GB}\Delta h_{ads.(i\to 1),0} + 2n\sum_i kTX^i_{GB}\ln\left(\frac{X^i_{GB}}{X^i_{Bulk}}\right) \tag{3}$$

where $\gamma^{(0)}_{GB}$ is the "clean" GB energy of the first component (without GB adsorption) and *n* is the number of atoms per unit area in the atomic plane parallel to the GB. This model has been used to numerically illustrate the high-entropy GB effect [26], where the GB energy can be reduced with increasing temperature when the bulk composition moves along the multicomponent solvus line (for a specimen saturated with many different segregating elements), as shown in Fig. 6 in Ref. [26].

To further illustrate the bulk high-entropy effect (that is distinct from the GB high entropy effect shown in Fig. 6 in Ref. [26]), we first conducted numerical experiments using a hypothetic, symmetrical, ideal, high-entropy solution of *N* matrix elements (M_i; $i = 1, 2, \ldots N$) and one segregating element (*S*), where stoichiometric line compounds (M_i)*S* can form to limit the solubilities (solvus curve). More details of the model and parameters used are described in the Supplementary Materials and the computed results are shown in Fig. 1(a). The inset of Fig. 1(a) shows that the solid solubility can be increased in the ternary system M_1-M_2-*S*, as compared with two binary subsystems, M_1-*S* and M_2-*S*. Subsequently, Fig. 1(a) shows that increasing *N* (the number of matrix elements M_i) results in more reduction in γ_{GB} and makes $d\gamma_{GB}/dT$ more negative to reduce the thermodynamic driving forces for grain growth at high temperatures. Furthermore, Fig. 1(b) shows the computed γ_{GB} *vs.* temperature curves for several cases, where the bonding and segregation energies were selected to represent the real Ni based alloys (see the Supplementary Material). Fig. 1(b) suggests that a $Ni_{29}Fe_{23}Co_{23}Cr_{23}Zr_2$ alloy will have substantially lower γ_{GB}, as compared with both a binary counterpart ($Ni_{93}Zr_7$) and the conventional high-entropy counterpart ($Ni_{25}Fe_{25}Co_{25}Cr_{25}$); here, only Zr is a strong segregating element (Supplementary Table S-I). Fig. 1(b) further suggests that adding two additional segregating elements, Nb and Mo, can further reduce γ_{GB} for a $Ni_{25}Fe_{23}Co_{23}Cr_{23}Mo_2Nb_2Zr_2$ alloy *via* a GB high-entropy effect, in addition to the bulk high-entropy effect to reduce γ_{GB}; this GB high-entropy effect is evident by the kink in the γ_{GB} *vs.* temperature curve in Fig. 1(b), below which more reduction in γ_{GB} and more negative $d\gamma_{GB}/dT$ are a result that both Zr and Nb are saturated so that the bulk composition moves along a ternary solvus line to

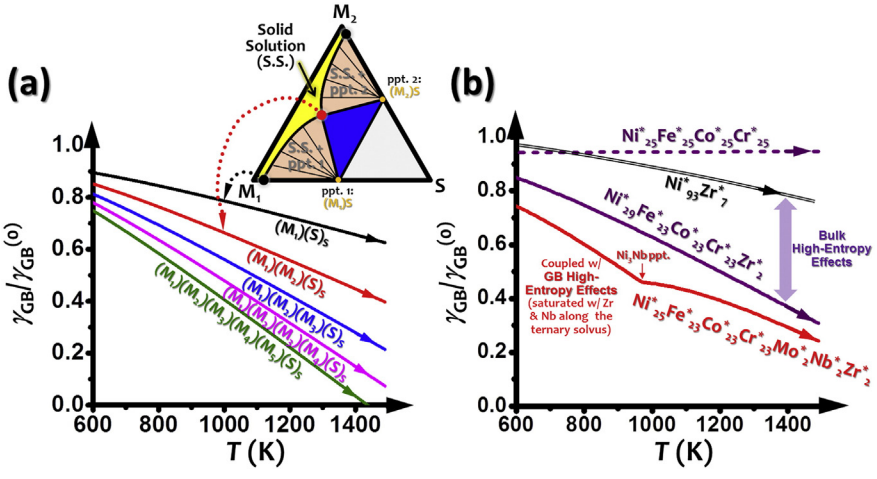

Fig. 1. (a) The computed $\gamma_{GB}/\gamma^{(0)}_{GB}$ *vs.* temperature curves along the bulk solvus curves for symmetrical ideal solutions of 1–5 matrix elements (M_i) and one segregating element (*S*). The subscript "$_S$" denotes that all specimens are saturated with element *S* at all temperatures (in equilibrium with *S*-enriched precipitates). The inset is an isothermal section of a ternary phase diagram, where the binary and ternary compositions on the solvus (labeled by the black and red dots) correspond to the specimen compositions for calculating the first two (black and red) curves. (b) The computed $\gamma_{GB}/\gamma^{(0)}_{GB}$ *vs.* temperature curves for several "Ni-like" alloys. Here, the superscripts "*" are used acknowledge that the calculations were conducted by using a lattice model with segregation enthalpies and bonding energies to represent real alloys, but with simplifications, to capture the most important trends. The model and parameters are described in the Supplementary Materials. (For interpretation of the references to color in this figure legend, the reader is referred to the web version of this article.)

Table 1
Measured grain sizes of various specimens.

Composition	Grain size measured by XRD (and TEM), nm		
	600 °C	900 °C	1000 °C
$Ni_{93}Zr_7$	25	>60 (189)	Coarse
$Ni_{25}Fe_{25}Co_{25}Cr_{25}$	43	Coarse	Coarse
$Ni_{29}Fe_{23}Co_{23}Cr_{23}Zr_2$	19	43	>60
$Ni_{25}Fe_{23}Co_{23}Cr_{23}Mo_2Nb_2Zr_2$	12.5	36 (43)	56
$Ni_{80}Mo_{6.6}Ti_6Nb_6Ta_{1.4}$	16	36 (32)	45

produce a GB high-entropy effect, as suggested in Ref. [26]. Subsequently, these four alloys discussed above were fabricated and examined; the experiments (discussed in detail later) supported the theories and modeling results.

An additional scheme/strategy to stabilize nanoalloys is to utilize kinetic effects, which is often coupled with the thermodynamic effects. Multicomponent segregation at GBs may maximize the solute-drag effects, which can be further enhanced through a so-called high-entropy "sluggish kinetics" effect [28,29]. First, a multicomponent alloy with different atomic sizes and bonding characteristics usually has local sites with a wider distribution of metastable energy levels (than those in unary and binary alloys). On one hand, when an atom jumps into a low-energy site, it can be trapped. On the other hand, if the site has a high energy, the atom has a higher chance to hop back to its original site so it does not contribute to diffusion effectively [29]. The combination of both scenarios may (on average) slow down the diffusion, as being demonstrated in the modeling of bulk diffusion in CoCrFeMnNi [30]; we believe that similar mechanisms may also slow down the migration of high-entropy GBs. Second, the diffusion rates of different elements in a GB with multicomponent adsorbates are different. Since the GB migration needs collective and cooperative diffusion of all adsorbates [31], grain growth may be pinned by the slowest segregating element. Similar sluggish kinetics effects have been demonstrated *via* diffusion-couple experiments in AlCoCrFeNi alloys [32]. Furthermore, Zener pinning can also play an important role to hinder the grain growth [33] and a multicomponent alloy may have more chances for effective Zener pinning by multiple (and different) precipitates that form at different temperatures. Finally, it is important to note that high-entropy GBs may also exhibit fast (instead of sluggish) kinetics in some other cases or under certain conditions. As one example of such possibilities, multicomponent segregation can promote GB disordering at high temperatures, which can in turn drastically increase interfacial kinetics (and potentially trigger abnormal grain growth [34]).

To test the proposed theories and strategies, nanoalloys were prepared *via* mechanical alloying. High-purity powders were well blended and sealed into a grinding vial in Ar atmosphere before high energy ball milling (HEBM; using a SPEX 8000D miller) for 20 h. Hardened steel

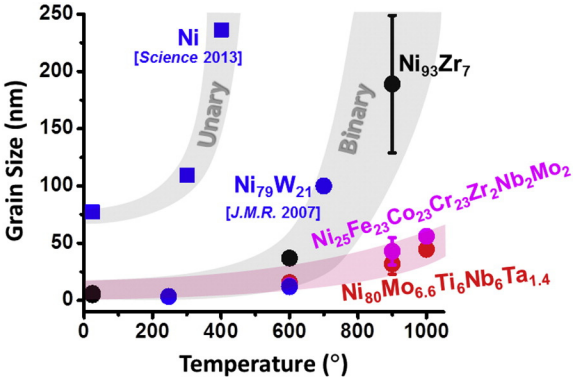

Fig. 3. Measured grain sizes *vs.* annealing temperatures curves for the $Ni_{93}Zr_7$, $Ni_{25}Fe_{23}Co_{23}Cr_{23}Mo_2Nb_2Zr_2$, and $Ni_{80}Mo_{6.6}Ti_6Nb_6Ta_{1.4}$ alloys made in this study, along with the curves for pure Ni [35] and $Ni_{79}W_{21}$ (representing the most stable binary Ni-based nanoalloy reported) [25] from literature for comparison.

grinding vials and balls were used. The ball-to-powder mass ratio was 5:1, with 1 wt.% stearic acid as processing control agent. The mechanically-alloyed specimens were annealed in Ar + 5% H_2 atmosphere at 600 °C, 900 °C and 1000 °C, respectively, for different durations (5 and 20 h). The specimens were examined by X-ray diffraction (XRD) and transmission electron microscopy (TEM).

XRD (Supplementary Fig. S1) showed that all specimens contain primarily an FCC phase, albeit the presence of small fractions of secondary phases in some cases. The grain sizes estimated by the Scherrer equation are presented in Table 1, which have been verified by direct TEM measurements for selected specimens (Fig. 2 and Supplementary Fig. S2).

The $Ni_{29}Fe_{23}Co_{23}Cr_{23}Zr_2$ nanoalloy exhibited a stable grain size of ~19 nm after annealing at 600 °C and ~43 nm after annealing at 900 °C, which outperformed the binary counterpart $Ni_{93}Zr_7$ (Table 1), as well as $Ni_{79}W_{21}$, the most stable binary Ni nanoalloy reported in literature [25] (Fig. 3). Moreover, a conventional high-entropy $Ni_{25}Fe_{25}Co_{25}Cr_{25}$ nanoalloy (for benchmarking) did not exhibit a stable nanoscale grain size at 900 °C (Table 1), showing that a pure high-entropy matrix is not sufficient for stabilizing nanoalloys at high temperatures. Finally, the $Ni_{25}Fe_{23}Co_{23}Cr_{23}Mo_2Nb_2Zr_2$ alloy, which may be benefited from both bulk and GB high-entropy effects (Fig. 1(b)), exhibited even better high-temperature stabilities at 900 °C and 1000 °C (Fig. 3; Table 1). These observed trends are consistent with the thermodynamic modeling results shown in Fig. 1(b); however, we wish to note that kinetic stabilization effects should also play important roles in preventing grain growth in all cases.

To further examine the kinetic effects, we designed a $Ni_{80}Mo_{6.6}Ti_6Nb_6Ta_{1.4}$ alloy, where the Ti, Nb, and Ta contents were

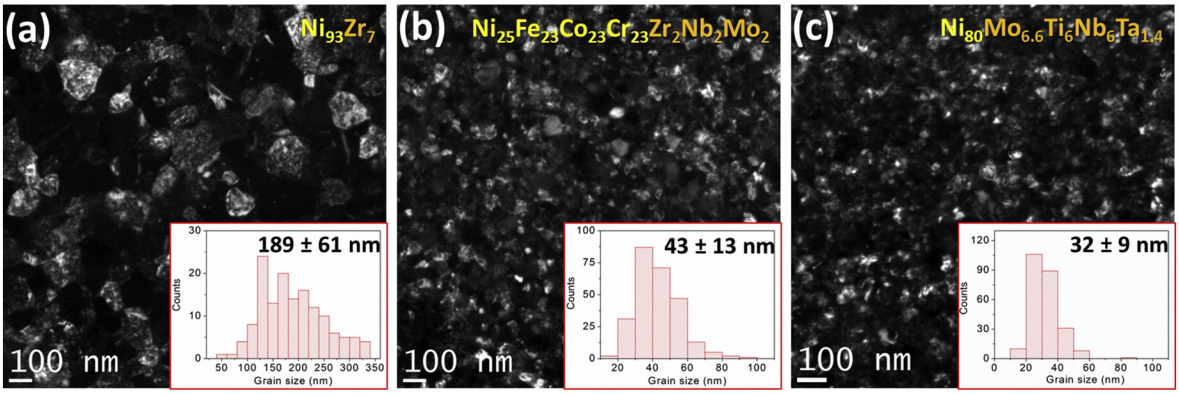

Fig. 2. Dark-field TEM images of the (a) $Ni_{93}Zr_7$, (b) $Ni_{25}Fe_{23}Co_{23}Cr_{23}Mo_2Nb_2Zr_2$, and (c) $Ni_{80}Mo_{6.6}Ti_6Nb_6Ta_{1.4}$ alloys after annealing at 900 °C for 5 h. The insets are the histograms of grain size distributions that were measured over 200 grains for each case.

about 60–70% of the binary solid solubility limits at 900 °C (Table S-II) while 6.6% Mo (*i.e.*, ~25% of binary solid solubility limit at 900 °C) was adopted to keep 80% of Ni. Thus, the thermodynamic effects on reducing GB energy should be less significant and the kinetic effects are presumably more important. The grain sizes were measured by XRD to be 16 nm, 36 nm, and 45 nm, respectively, for the $Ni_{80}Mo_{6.6}Ti_6Nb_6Ta_{1.4}$ specimens annealed at 600 °C, 900 °C, and 1000 °C, respectively (Table 1), representing a substantial improvement to binary nanoalloys (Fig. 3) and being in par with what have been achieved for the $Ni_{25}Fe_{23}Co_{23}Cr_{23}Mo_2Nb_2Zr_2$ nanoalloy (Table 1). We do recognize that it is almost impossible to know how much the stabilization is in fact due to kinetics (*vs.* thermodynamics); in most cases (including this instance), the stabilization should be a result of combined thermodynamic and kinetics effects.

We also characterized selected specimens with TEM (Fig. 2), where the grain sizes of the $Ni_{25}Fe_{23}Co_{23}Cr_{23}Mo_2Nb_2Zr_2$ and $Ni_{80}Mo_{6.6}Ti_6Nb_6Ta_{1.4}$ alloys annealed at 900 °C were measured to be 43 ± 13 and 32 ± 9 nm, respectively, which are in good agreement with the XRD measurements (Table 1). In comparison, the grain size of the binary $Ni_{93}Zr_7$ alloy was measured to be 189 ± 61 nm by TEM. The dark-field TEM images in Fig. 2 (as well as Supplementary Fig. S2) also show that the grains are homogeneous without any abnormally-large grains. The histograms of grain size distributions are shown in Figs. 3 and S2.

In summary, this study proposed and tested several new theories and strategies to utilize high-entropy GB complexions to enhance the thermal stability of nanocrystalline alloys at high temperatures. First, we demonstrated, *via* numerical experiments, that GB energies could be reduced *via* bulk and/or GB high-entropy effects at/within the solid solubility limit to reduce the thermodynamic driving force for grain growth at high temperatures. Moreover, grain growth can be hindered by the high-entropy sluggish kinetics at GBs. To test these new theories, several nanoalloys were designed and fabricated to demonstrate outstanding thermal stabilities. Specifically, Fig. 3 compares our results with the reported grain sizes for nanocrystalline pure Ni [35] and $Ni_{79}W_{21}$ [25]. For pure Ni, the grains started to coarsen at 300–400 °C. When Ni was alloyed with W, the coarsening temperature was improved to 600–700 °C [36]. In this study, we successfully stabilized a Ni-based $Ni_{80}Mo_{6.6}Ti_6Nb_6Ta_{1.4}$ alloy and a Ni-containing high-entropy $Ni_{25}Fe_{23}Co_{23}Cr_{23}Mo_2Nb_2Zr_2$ alloy up to 1000 °C *via* an innovative use of high-entropy GB complexions thru both thermodynamic and kinetic effects. This study provides a new pathway to stabilize nanocrystalline alloys at high temperatures, which can also be applied a broad range of other materials.

Acknowledgement

We gratefully acknowledge the financial support from an Office of Naval Research MURI program (grant no. N00014-11-1-0678; managed by Dr. David Shifler).

Appendix A. Supplementary data

Supplementary data to this article can be found online at http://dx.doi.org/10.1016/j.scriptamat.2016.07.014.

References

[1] H. Gleiter, Acta Mater. 48 (2000) 1–29.
[2] L. Lu, X. Chen, X. Huang, K. Lu, Science 323 (2009) 607–610.
[3] Y. Wang, M. Chen, F. Zhou, E. Ma, Nature 419 (2002) 912–915.
[4] Y.H. Zhao, X.Z. Liao, S. Cheng, E. Ma, Y.T. Zhu, Adv. Mater. 18 (2006) 2280–2283.
[5] H. Gleiter, Prog. Mater. Sci. 33 (1989) 223–315.
[6] R. Birringer, Mater. Sci. Eng. A 117 (1989) 33–43.
[7] B. Günther, A. Kumpmann, H.D. Kunze, Scr. Metall. Mater. 27 (1992) 833–838.
[8] C.E. Krill, H. Ehrhardt, R. Birringer, Z. Metallkd. 96 (2005) 1134–1141.
[9] C.C. Koch, R.O. Scattergood, K.A. Darling, J.E. Semones, J. Mater. Sci. 43 (2008) 7264–7272.
[10] M. Tschopp, H. Murdoch, L. Kecskes, K. Darling, JOM 66 (6) (2014) 1000–1019.
[11] A.R. Kalidindi, T. Chookajorn, C.A. Schuh, JOM 67 (12) (2015) 2834–2843.
[12] H. Höfler, R. Averback, Scr. Metall. Mater. 24 (1990) 2401–2406.
[13] Z. Gao, B. Fultz, Nanostruct. Mater. 4 (1994) 939–947.
[14] A. Michels, C. Krill, H. Ehrhardt, R. Birringer, D. Wu, Acta Mater. 47 (1999) 2143–2152.
[15] J. Weissmüller, Nanostruct. Mater. 3 (1993) 261–272.
[16] J. Weissmüller, J. Mater. Res. 9 (1994) 4–7.
[17] R. Kirchheim, Acta Mater. 50 (2002) 413–419.
[18] P.R. Cantwell, M. Tang, S.J. Dillon, J. Luo, G.S. Rohrer, M.P. Harmer, Acta Mater. 62 (2014) 1–48.
[19] B.K. VanLeeuwen, K.A. Darling, C.C. Koch, R.O. Scattergood, B.G. Butler, Acta Mater. 58 (2010) 4292–4297.
[20] T. Chookajorn, H.A. Murdoch, C.A. Schuh, Science 337 (2012) 951–954.
[21] K. Darling, B. VanLeeuwen, C.C. Koch, R.O. Scattergood, Mater. Sci. Eng. A 527 (2010) 3572–3580.
[22] K.A. Darling, R.N. Chan, P.Z. Wong, J.E. Semones, R.O. Scattergood, C.C. Koch, Scr. Mater. 59 (2008) 530–533.
[23] A. Khalajhedayati, Z. Pan, T.J. Rupert, Nat. Commun. 7 (2016) 10802.
[24] L. Li, M. Saber, W. Xu, Y. Zhu, C.C. Koch, R.O. Scattergood, Mater. Sci. Eng. A 613 (2014) 289–295.
[25] A.J. Detor, C.A. Schuh, J. Mater. Res. 22 (2007) 3233–3248.
[26] N. Zhou, T. Hu, J. Luo, Curr. Opinion Solid State Mater. Sci. (2016), http://dx.doi.org/10.1016/j.cossms.2016.05.001 (published online).
[27] P. Wynblatt, D. Chatain, Metall. Mater. Trans. 37A (2006) 2595–2620.
[28] Z.P. Lu, H. Wang, M.W. Chen, I. Baker, J.W. Yeh, C.T. Liu, T.G. Nieh, Intermetallics 66 (2015) 67–76.
[29] S. Praveen, J. Basu, S. Kashyap, R.S. Kottada, J. Alloys Compd. 662 (2016) 361–367.
[30] K.Y. Tsai, M.H. Tsai, J.W. Yeh, Acta Mater. 61 (2013) 4887–4897.
[31] G. Gottstein, L.S. Shvindlerman, Grain Boundary Migration in Metals: Thermodynamics, Kinetics, Applications, CRC express, Florida, 1999.
[32] J. Dąbrowa, W. Kucza, G. Cieślak, T. Kulik, M. Danielewski, J.-W. Yeh, J. Alloys Compd. 674 (2016) 455–462.
[33] R.D. Doherty, D.A. Hughes, F.J. Humphreys, J.J. Jonas, D.J. Jensen, M.E. Kassner, W.E. King, T.R. McNelley, H.J. McQueen, A.D. Rollett, Mater. Sci. Eng. A 238 (1997) 219–274.
[34] V.K. Gupta, D.-H. Yoon, H.M. Meyer Iii, J. Luo, Acta Mater. 55 (2007) 3131–3142.
[35] X.C. Liu, H.W. Zhang, K. Lu, Science 342 (2013) 337–340.
[36] A.J. Detor, C.A. Schuh, Acta Mater. 55 (2007) 4221–4232.